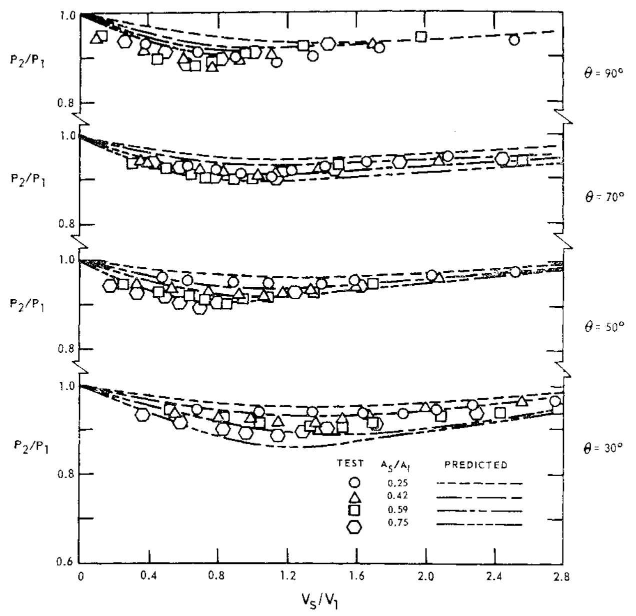

Fig. 6 Downstream and upstream static pressure ratios.

pressure ratios is that the experimental results do not approach unity as $\dot{m}_s/\dot{m}_1 \rightarrow 0$. This is caused by vortex action generated from a combination of misalignment and slight differences in the diameters of the upstream and downstream tubes in the secondary injection device. These effects are accentuated by the small size of the experimental system, and more accurate results would be expected with a larger system.

Figure 6 shows that the effects of changes in A_s/A_1 on P_2/P_1 increases as θ decreases. This figure also indicates trends similar to those discussed for Fig. 5 as $\dot{m}_s/\dot{m}_1 \rightarrow 0$. The curves of T_2/T_1 (not shown) are of similar character. The temperature variations are small across the injection region, thus the velocity ratios shown in Fig. 5 essentially represent Mach number ratios.

Conclusions

In summary, this study indicates that: 1) the primary flow upstream of the injection slot is essentially unaffected by the secondary injection; 2) the aerodynamic interaction between the flow streams is completed within $x/D_1 = 2$; 3) the flow separation in the mixing region is a strong function of θ; 4) the results of Refs. 4 and 7 indicate general flowfield characteristics that disagree with the experimental results of this study and the water-table results of Glick and Thurman[2]; 5) the analysis of Glick et al.[3] yields incorrect results because it allows a downstream flow area greater than the tube cross-sectional area; 6) the present analysis has wider application than that of Ref. 2 because it does not depend on a known value of P_{min}; 7) the velocity increase across the mixing region is strongly dependent on V_s/V_1; 8) changes in P and P_o across the injection region are not strong functions of θ or A_s/A_1; and 9) temperature changes across the injection region are small.

References

[1] Zumwalt, G. W. and Jackomis, W. N., "A Secondary Injection Nozzle for Solid Rocket Thrust Magnitude Control," paper 2337-62, 1962, American Rocket Society.

[2] Glick, R. L. and Thurman, J. L., "An Analysis of the Circumferential Slot Effects on the Internal Ballistics of the TX354 Motor," Special Rept. U-65-11A, Feb. 1965, Thiokol Chemical Corp., Huntsville, Ala.

[3] Glick, R. L., Caveny, L. H., and Thurman, J. L., "Internal Ballistics of Slotted-Tube, Solid Propellant Rocket Motors," *Journal of Spacecraft and Rockets*, Vol. 4, No. 4, April 1967, pp. 525–530.

[4] Maegley, W. J., "An Optical Study of the Injection of a Gas Into the Throat Region of an Air Nozzle," M.S. thesis, 1963, Oklahoma State Univ., Stillwater, Okla.

[5] Walker, R. E., Stone, A. R., and Shandor, M., "Secondary Gas Injection in a Conical Rocket Nozzle," *AIAA Journal*, Vol. 1, No. 2, Feb. 1963, pp. 334–338.

[6] Broadwell, J. E., "Analysis of the Fluid Mechanics of Secondary Injection for Thrust Vector Control," *AIAA Journal*, Vol. 1, No. 5, May 1963, pp. 1067–1075.

[7] Stutzman, R. D., "Investigation of Secondary Injection Using the Hydraulic Analogy," unpublished Rept., 1963, School of Mechanical Engineering, Oklahoma State Univ., Stillwater, Okla.

Effective Sky Temperatures for Several Martian Atmospheric Models

JOSEPH P. WACHTER*
Martin Marietta Corporation, Denver, Colo.

Nomenclature

A	=	total cm-atm of CO_2 in the Martian atmosphere
B_ν	=	blackbody hemispherical flux at wave number ν, gcal/cm² day
n	=	number of atmospheric layers in model
P, P_{eff}	=	pressure and effective pressure, mb
P^*	=	average pressure in the interval dP from Eq. (3)
Q	=	downward atmospheric heat flux, gcal/cm² day
R	=	$R(u, t) = \int (dB_\nu/dT)(1 - \tau_f)d\nu$
T^*	=	temperature taken from an atmospheric model for the pressure P^*, °K
T	=	temperature taken from an atmospheric model for the pressure P, °K; T_i, for P^*, °K
T_{sky}	=	effective sky temperature, °K
ΔT	=	temperature difference across an atmospheric layer
u	=	reduced path length of CO_2 measured by the height in cm of a column of CO_2 reduced to standard temperature and pressure, cm
α_x	=	volumetric percentage of species x
ν	=	wave number, frequency/(speed of light)
σ	=	Stefan-Boltzman constant
τ_f	=	transmissivity function[1,2]
$\langle\ \rangle$	=	evaluated at the average pressure of an atmospheric layer

Subscripts

s	=	conditions at the planetary surface
t	=	conditions at the top of the atmosphere

Introduction

THE thermal analysis of a Martian lander and the design of Mars surface environmental simulators require the calculation of the downward radiation flux from the Martian atmosphere. This may be expressed in terms of an effective sky temperature T_{sky}, defined as the temperature of a blackbody emitting the same total downward flux as the atmosphere. It is a function of the orientation of the receiving surface, composition and temperature profile of the atmosphere, and the effective thickness of the absorbing gases.

The downward heat flux can be calculated using the method of Elsasser.[1,2] Ohring[3] applied Elsasser's method to determine the atmospheric radiation flux while determining the Mars surface temperature. However, the atmospheric model Ohring used is substantially different from current models. Other studies of the Martian atmosphere have not provided

Received October 13, 1969. This work was done as part of an internally funded Martin Marietta Corporation research program.

* Engineer, Thermal Control Section, Propulsion and Mechanical Engineering Department. Member AIAA.

Table 1 Description of Martian atmospheric models and their effective sky temperatures

Atmospheric model	Composition, volumetric percentage CO_2	N_2	Ar	P_s,mb	ΔP, mb	T_s,°K	T_{sky},°K
Viking engineering model[8]							
Minimum surface density	100	0	0	4	0.125	280	168.6
Minimum surface density scale height					0.2	180	100.7
Most probable	68.5	18.5	13	9	0.25	230	142.9
Maximum surface density	19	60	21	20	0.50	180	107.7
Maximum surface density scale height					0.50	280	176.7
JPL lower atmosphere model I[6]	80	10	10	10	0.2	180	111.9
						210	131.9
						230	145.4
						290	183.2

the data necessary for thermal analysis of landers or simulators. These data are provided here in the form of T_{sky}'s for several current Mars atmospheric models.

There is no simple correlation for T_{sky} as a function of the zenith angle formed by the normal to the receiving surface; T_{sky} is a minimum for a horizontal flat plate and a maximum for a vertical plate. It is assumed herein that the planet is flat with a stratified atmosphere, and the receiving surface is a horizontal flat plate. Following Ohring and Mariano,[4,5] CO_2 is the only absorbing gas considered. Although there may be small amounts of water vapor and ozone present, the atmospheric absorption due to them is negligible. Nitrogen and argon are assumed to be the only other components of the atmosphere. No variation of atmospheric composition with altitude was considered.

Implicit in the use of Elsasser's radiation model is the assumption of the Lorentz line shape for the far infrared absorption lines. The line shape (absorption coefficient as a function of frequency for a single spectral line) is determined by two processes, Lorentz line broadening and Doppler line broadening. Lorentz broadening is due to molecular collisions whereby the frequency of the emission is slightly changed by intermolecular forces during an encounter by the radiating molecule. Doppler broadening is due to the molecular motion of the radiating molecules. The relative importance between the two processes depends on the pressure, temperature, and concentration of the absorbing gases. Ohring and Mariano[4] checked the Lorentz assumption for the Martian atmosphere and concluded that the neglect of the Doppler broadening is justified.

Method of Computation

Following Elsasser[1,2] the downward thermal flux at the bottom of an atmosphere is given by

$$Q = -\int_{T_s}^{T_t} R(u,T)dT + \int_0^{T_t} R(u_t,T)dT =$$

$$\sum_{i=1}^{n} - R\,(\langle u_i\rangle,\langle T_i\rangle)\Delta T + \int_0^{T_t} R(u_t,T)dT \quad (1)$$

The effective sky temperature is given by

$$T_{sky} = (Q/\sigma)^{1/4} \quad (2)$$

Tables of $R(u,T)$ for $193°K \leqslant T \leqslant 313°K$ and tables of

$$\int_0^{193} R(u,T)\,dT$$

as a function of log u are given by Elsasser[2] for CO_2.

The increment of the reduced path length across a pressure interval dP is given by

$$du = (A/P_s)(P_{eff}/1000)(273/T^*)^{1/2}dP \quad (3)$$

The different amounts of line broadening caused by the presence of several species are accounted for by the use of an effective pressure P_{eff}. Carbon dioxide self-broadening is 1.3 times as effective as nitrogen broadening, whereas argon broadening is 0.78 times as effective.[6,7] Thus, for the assumed constituents of the Martian atmosphere,

$$P_{eff} = P^*(1.0 + 0.3\alpha_{CO_2} - 0.22\alpha_{Ar}) \quad (4)$$

Since Lorentz broadening is due to molecular collisions, it is necessary to use volumetric percentages, α_x, in the calculation of P_{eff}.

The integrals in Eq. (1) were evaluated numerically by dividing the atmosphere into layers of equal pressure increments ΔP given in Table 1. The last layer at the top of the atmosphere was subdivided into 15 pressure intervals to insure convergence of the integral in this region.

The tables of $R(u,T)$ were extrapolated to lower temperatures where necessary by noting that $R(u,O) = 0$ and checked using the tabulated integrals given by Elsasser.[2] Linear interpolation on log u and temperature were used in the $R(u,T)$ tables. Also,

$$\int_0^{T_t} R(u_t,T)dT = \left[\frac{T_t}{193}\right]^4 \int_0^{193} R(u_t,T)dT$$

was assumed.

The reduced path length is defined as zero at the planetary surface. Eq. (2) was integrated numerically for each atmospheric layer, integrating from the surface to the average pressure of the layer.

Results

The five model atmospheres from the Viking Project Mars Engineering Model[8] and the Jet Propulsion Laboratory (JPL) Lower Atmosphere Model I[9] for four surface temperatures were considered. All of these atmospheric models were developed for preliminary design purposes and do not include the results of the 1969 Mariner flights. The atmospheric compositions, surface pressures, pressure differences across layers, surface temperatures, and the effective sky temperatures are presented in Table 1.

References

[1] Elsasser, W. M., *Heat Transfer by Infrared Radiation in the Atmosphere, Harvard Meteorological Studies No. 6*, Blue Hill Meteorological Observatory, Harvard Univ., Milton, Mass., 1942, pp. 1–107.

[2] Elsasser, W. M., *Atmospheric Radiation Tables, Meteorological Monographs*, Vol. 4, No. 23, American Meteorological Society, Boston, Mass., 1960, pp. 1–43.

[3] Ohring, G., Tang, W., and DeSanto, G., "Theoretical Estimates of the Average Surface Temperature on Mars," *Journal of the Atmospheric Sciences*, Vol. 19, Nov. 1962, pp. 444–449.

[4] Ohring, G. and Mariano, J., "Seasonal and Latitudinal Variations of the Average Surface Temperature and Vertical Temperature Profile on Mars," *Planetary Meteorology*, GCA-TR-67-5-N, March 1967, GCA Corp., Bedford, Mass., pp. 1–38.

[5] Ohring, G. and Mariano, J., "The Vertical Temperature Distribution in the Martian Atmosphere," *Journal of the Atmospheric Sciences*, Vol. 23, No. 2, March 1966, pp. 251–255.

[6] Gray, L. D., "Transmission of the Atmosphere of Mars in the Region of 2 μ" *Icarus*, Vol. 5, No. 4, July 1966, pp. 390–398.

[7] Gray, L. D., private communication, 1969, Jet Propulsion Lab., Pasadena, Calif.

[8] Michael, Jr., W. H., Wood, G. P., and Young, A. T., "Viking Project Mars Engineering Model," M73-106-0, Feb. 1969, Viking Project Office, NASA Langley Research Center, Hampton, Va.

[9] Jet Propulsion Laboratory Lunar and Planetary Sciences Section Staff, "Mars Scientific Model," JPL Document 606-1, Vol. 1, July 1968, Jet Propulsion Lab., Pasadena, Calif., Sec. 5.1, pp. 1–13, Sec. 5.2, pp. 1–11, Sec. 5.3, pp. 1–22.

Application of the Line-Source Technique for Vacuum Thermal Conductivity Measurements

Lawrence R. Greenwood*
NASA Langley Research Center, Hampton, Va.

and

Robert A. Comparin†
Virginia Polytechnic Institute, Blacksburg, Va.

THE space environment can alter the thermal and mechanical properties of engineering materials.[1] Properties must be measured in the environment of interest (i.e., in situ) to obtain valid results.[2] The necessity of making in situ measurements of thermal conductivity in a variety of environments (e.g., vacuum, planetary atmospheres) led to an evaluation of available techniques for this application. The conventional techniques, such as the guarded hot plate and comparator, are not well suited for environmental studies because the large contact areas between a heater plate and the sample could alter the interaction with the surrounding environment. The line-source technique appears to be well suited for making in situ measurements in a variety of environments, because the measuring apparatus is inside the sample, and all surfaces are free to interact with the surrounding environments. There are little data available, however, on the accuracy of this technique, or on its use in vacuum. This Note presents the results of a recent study wherein 1) the accuracy of the line-source technique was established for application to an ablative heat-shield material, and 2) the technique was applied to make vacuum thermal conductivity measurements.

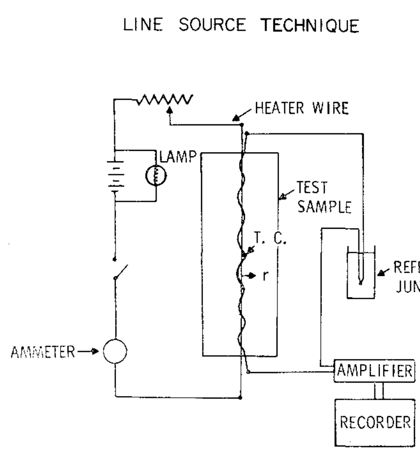

Fig. 1 Line-source technique for measuring thermal conductivity.

Line-Source Technique

A heater wire and thermocouple are placed inside the sample as shown in Fig. 1. Application of the equation for heat conduction with an instantaneous line-source leads to

$$K = [q/4\pi(\theta_2 - \theta_1)] \ln(t_2 - t_0)/(t_1 - t_0) \qquad (1)$$

where K = thermal conductivity, q = heat input, θ = temperature, t = time after initiation of heat generation, and t_0 = correction factor.

The assumptions necessary to solve the basic differential equation of conduction to obtain Eq. (1) include: 1) a semi-infinite heat sink (i.e., no change in the sample surface temperature), 2) no heat loss at the sample ends, 3) a heat source that is vanishingly small, and 4) an instantaneous heat input at time zero. The integration of the basic differential equation results in a series solution, and to obtain Eq. (1) the assumption is made that $r^2/4\alpha t$ is very small, where r is the radial distance from the center line of the sample to the point where the temperature changes are measured, and α is the thermal diffusivity. A detailed discussion of the assumptions involved is given in Ref. 3.

In the experimental application of Eq. (1) to measure thermal conductivity, the assumed conditions can only be approximated, and departures from these initial assumptions result in errors. When log$t$ vs temperature (θ) is plotted for a line-source measurement, Eq. (1) indicates that the resulting curve should be linear. However, since the assumed conditions can only be approximated, a plot of the experimental data will deviate from a straight line. Errors due to assumption (1) can be made negligible by a proper combination of sample size and test time.

Van der Held and Van Drunen[3] have shown that the error due to assumptions can be eliminated by including the t_0 correction factor, a constant which must be determined experimentally for each sample. A number of researchers have proposed methods of determining t_0, but all methods are difficult to apply and introduce uncertainties into the thermal conductivity calculations.

Since the value of t_0 is independent of time, it is apparent that the influence of t_0 on K becomes less as the test time in-

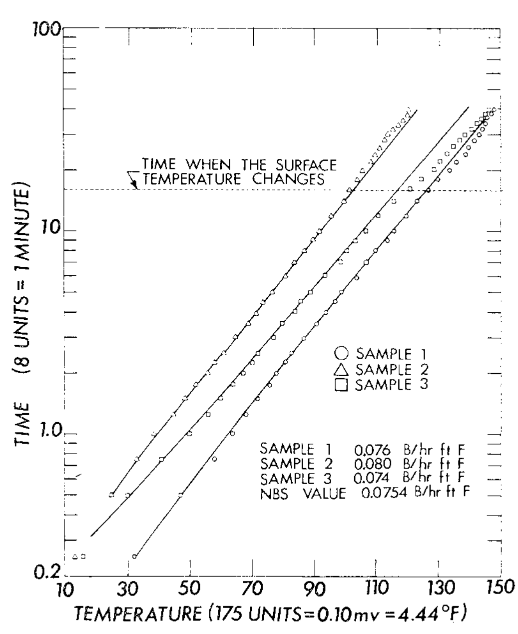

Fig. 2 Temperature variation with time at atmospheric pressure.

Presented as Paper 69-1013 at the AIAA/ASTM/IES 4th Space Simulation Conference, Los Angeles, Calif., September 8–10, 1969; submitted September 29, 1969; revision received November 10, 1969.

* Head, Space Vacuum Laboratory Section. Associate AIAA.
† Professor, Mechanical Engineering Department. Member AIAA.